Analytical prediction of the segregation of inertial particles in turbulent flows

By M. Esmaily-Moghadam AND A. Mani

1. Motivation and background

A detailed understanding of the dynamics of dispersed particles in turbulent flows is essential for a wide range of applications, from the physics underlying rain formation to the efficient operation and design of particle-based solar receivers. Such understanding is the basis of any modeling effort aimed at weather forecast or engineering design. A wide range of applications in science and engineering, such as planet formation, sediment transport in environmental flows, and pharmaceutical applications, benefit from an accurate modeling of particle-laden flows (Eaton & Fessler 1994; Balachandar & Eaton 2010).

The behavior of particles in turbulent flows varies significantly depending on the density ratio of particle to carrier flow, the particle volume fraction, the size of particles in relation to the characteristic length scale of the flow, the particle shape, the underlying flow, the volumetric forcing, and the presence of solid boundaries. In this study, we focus on a part of the parameter space in which particles are much denser than the fluid, the volume and mass fractions are much smaller than 1, the particles are spherical and much smaller than the smallest length scale of the flow, flow is isotropic and no solid boundary or body force is present. For such a simplified case, the high density ratio allows the history terms in the particle equation of motion to be neglected, the small volume and mass fractions allow the effect of particles on flow and particle-particle interactions to be neglected, the small particle size in combination with the absence of shape effects allows finite size effects to be neglected, and an isotropic flow in the absence of body force allows the system to be expressed in a canonical form that depends on a limited number of nondimensional parameters.

The behavior of the simplified system described above still remains fairly complex. In particular, depending on the time scale of particles in relation to the characteristic time scale of the flow, generally denoted by the Stokes number, particles may homogeneously disperse in space or preferentially concentrate in certain regions of the flow. Particle segregation in such a canonical flow has been the subject of several studies in the past. It has been observed experimentally (Fessler *et al.* 1994; Aliseda *et al.* 2002; Salazar *et al.* 2008; Saw *et al.* 2008), simulated numerically (Ray & Collins 2011; Calzavarini *et al.* 2008; Tagawa *et al.* 2012; Goto & Vassilicos 2008), and described analytically (Maxey 1987; Robinson 1956; Bec *et al.* 2004). In the present study, we focus on the analytical description of this system and employ numerical simulations for verification purposes.

The degree to which particles segregate in a turbulent flow strongly depends on the particle Stokes number. We define the Stokes number as the ratio of particle relaxation time $\tau = \rho_\mathrm{p} d_\mathrm{p}^2/(16\rho_\mathrm{f}\nu)$ to the Kolmogorov time scale $\tau_\eta = \sqrt{(}\nu/\epsilon)$, in which ρ_p is the particle density, d_p is the particle diameter, ρ_f is the fluid density, ν is the fluid kinematic viscosity, and ϵ is the mean volumetric dissipation rate. It has been shown that $\mathrm{St} = \tau/\tau_\eta \ll 1$ particles become neutral fluid tracers and experience minimum segregation.

There is also minimal segregation at the limit of $\mathrm{St} \gg 1$, where particles follow a ballistic trajectory uncorrelated with the underlying flow. The maximum segregation is achieved when $\mathrm{St} = \mathcal{O}(1)$. The non-monotonic variation of particle segregation versus St has been observed experimentally and numerically. However, this is yet to be described analytically.

One of the first analytical relations for quantification of particle segregation was obtained by Robinson (1956) and Maxey (1987). This relation, which hereafter is referred to as R-M, is obtained by approximating the acceleration of particles with that of flow. Denoting the position of a particle by $\boldsymbol{x}(t)$ and the flow velocity at the particle location by $u(\boldsymbol{x}, t)$, the nondimensionalized equation of the motion of a particle subjected to the Stokes drag is

$$\ddot{\boldsymbol{x}} = \boldsymbol{u}(\boldsymbol{x}, t) - \dot{\boldsymbol{x}}, \tag{1.1}$$

where $\dot{(\bullet)} := \mathrm{d}(\bullet)/\mathrm{d}t$. We employed τ, L, and $U = L/\tau$ as the time, length, and velocity scales to nondimensionalize corresponding parameters in Eq. (1.1). All the following equations are also nondimensionalized based on τ and L. τ is the particle relaxation time, defined above, and L is a characteristic length scale. The following formulations and the end result do not depend on the choice of L. The complexity of Eq. (1.1) is a result of the dependence of $\boldsymbol{u}$ on $\boldsymbol{x}$ that leads to its nonlinear behavior. Following R-M derivation by approximating $\ddot{\boldsymbol{x}} \approx \mathrm{D}\boldsymbol{u}/\mathrm{Dt}$ and assuming $\nabla \cdot \boldsymbol{u} = 0$, i.e. flow being incompressible, and taking the divergence of Eq. (1.1), we obtain

$$\mathcal{C} := \overline{\nabla \cdot \dot{\boldsymbol{x}}} = \overline{\|\boldsymbol{\Omega}\|^2 - \|\boldsymbol{S}\|^2}, \tag{1.2}$$

where $\boldsymbol{\Omega}$ and $\boldsymbol{S}$ are the nondimensional rotation-rate and strain-rate and $\overline{(\bullet)}$ denotes Lagrangian time-averaging over the trajectory of a particle. The R-M relation relates the degree of preferential concentration to the divergence of particle velocity field, here defined as $\mathcal{C}$. Denoting a collection of inertial particles that are within an infinitesimal distance from each other as a cloud of particles, $\mathcal{C}$ is the exponential rate at which the volume of the cloud changes over a long period. In what follows, we adopt $\mathcal{C}$ for characterization of the particle segregation.

Approximating the acceleration of particles with that of flow strictly limits the validity of R-M to small St. The accuracy of R-M in predicting the first- and second-order statistics of $\mathcal{C}$ has been shown for $\mathrm{St} < 1$ in homogeneous turbulence (Ferry *et al.* 2003; Esmaily & Mani 2016) as well as synthetic flows (Ijzermans *et al.* 2010). For $\mathrm{St} \geq 1$, R-M predicts an unbounded $\mathcal{C}$ proportional to St, hence failing to capture the non-monotonic behavior of $\mathcal{C}(\mathrm{St})$.

In Esmaily & Mani (2016), we derived an alternative relationship for $\mathcal{C}$ that is the first-order correction to R-M. In that study, we linearized Eq. (1.1) and expressed $\boldsymbol{u}$ in the Fourier space to obtain an eigenvalue problem for the Lyapunov exponents of pairs of inertial particles. The sum of these exponents (in three dimensions λ_1, λ_2, and λ_3) is equal to the divergence of the particle velocity field, $\mathcal{C}$. We showed that $\mathcal{C}$ can be expressed as

$$\mathcal{C} = \int_{-\infty}^{\infty} \frac{\tilde{\rho}^{\mathrm{Q}}(\omega)}{1+\omega^2} \mathrm{d}\omega, \tag{1.3}$$

where

$$\tilde{\rho}^{\mathrm{Q}}(\omega) := \frac{1}{2\pi} \int_{-\infty}^{\infty} \rho^{\mathrm{Q}}(t) e^{-\hat{\imath}\omega t} \mathrm{d}t = \frac{1}{2\pi} \int_{-\infty}^{\infty} \mathrm{tr}\left(-\overline{\nabla \boldsymbol{u}(t') \nabla \boldsymbol{u}(t'+t)}\right) e^{-\hat{\imath}\omega t} \mathrm{d}t. \tag{1.4}$$

ρ^{Q} is half of the autocovariance of the Q-criterion, defined in the literature for identi-

fication of the vortical regions (Hunt *et al.* 1988; Dubief & Delcayre 2000). Its Fourier transformation $\tilde{\rho}^{\mathrm{Q}}(\omega) = \tilde{\rho}^{\Omega}(\omega) - \tilde{\rho}^{\mathrm{S}}(\omega)$, where $\tilde{\rho}^{\Omega}$ and $\tilde{\rho}^{\mathrm{S}}$ are the Fourier transformation of the rotation-rate and strain-rate autocovariance functions, respectively. Hence, the sign of $\tilde{\rho}^{\mathrm{Q}}$ indicates dominance of flow rotation-rate ($\tilde{\rho}^{\mathrm{Q}} > 0$) and strain-rate ($\tilde{\rho}^{\mathrm{Q}} < 0$), which are associated with elliptic and hyperbolic regions of the flow, respectively. Note these functions are computed along the trajectory of the particles, are different from a Eulerian averaged quantity, and thus are dependent on St.

The primary assumption associated with Eq. (1.3), which we refer to as S-L hereafter, is that the Lyapunov exponents λ_i are much smaller than 1. This assumption is valid at relatively small St in which λ_i are also small. In Esmaily & Mani (2016) we also showed S-L exactly reproduces R-M as $\mathrm{St} \to 0$. At this limit, ω^2 in the denominator of Eq. (1.3) can be neglected, thus reproducing Eq. (1.2). A comparison against the direct computations over a wide range of St showed that S-L and R-M provide accurate predictions for small St. At higher St, although S-L remains bounded and provides a better prediction than R-M does, it still deviates from the exact calculations due to the underlying assumption of $|\lambda_i| \ll 1$.

The objective of this study is to propose an analytical relationship for $\mathcal{C}(\tilde{\rho}^{Q})$ that is valid at both small and large St. In what follows, we present a step-by-step derivation of an asymptotic solution, extracted from the linearized form of Eq. (1.1). Then, we compare the prediction of R-M, S-L, and our solution to the exact computations. For this purpose, we consider a one-dimensional single-mode oscillatory flow. Through this case, we test the accuracy of the proposed solution and discuss its implications. The assessment of the present analysis in more complex flows remains a subject for future studies.

2. Analytical derivation

In this section, the derivation of our asymptotic solution to Eq. (1.1) is presented. To begin, we define the trajectory of a particle that is located at $\boldsymbol{X}$ at time $t = 0$ as $\boldsymbol{x} = \boldsymbol{x}(\boldsymbol{X}, t)$. The trajectory of a nearby particle initially located at $\boldsymbol{X} + \delta\boldsymbol{X}$ is then described by $\boldsymbol{x}(\boldsymbol{X} + \delta\boldsymbol{X}, t) = \boldsymbol{x}(\boldsymbol{X}, t) + (\partial\boldsymbol{x}/\partial\boldsymbol{X})\delta X$. The deformation tensor associated with this motion is

$$\boldsymbol{J} := \frac{\partial \boldsymbol{x}}{\partial \boldsymbol{X}}. \tag{2.1}$$

The determinant of $\boldsymbol{J}$, denoted by $|\boldsymbol{J}|$, can be interpreted as the volume of a cloud of particles relative to its initial volume that undergo a linear deformation characterized by $\boldsymbol{J}$. Therefore, defining $\mathcal{C}^t$ as the finite-time exponential rate of change of the volume of the cloud, viz.

$$\mathcal{C}^t := \frac{\ln|\boldsymbol{J}(t+t')| - \ln|\boldsymbol{J}(t')|}{t}. \tag{2.2}$$

Then, following our earlier definition of $\mathcal{C}$, we have

$$\mathcal{C} = \lim_{t\to\infty} \mathcal{C}^t. \tag{2.3}$$

Based on Eqs. (2.2) and (2.3), $\mathcal{C}$ can be computed from $\boldsymbol{J}$. To obtain a relationship for $\boldsymbol{J}$, we take the derivative of Eq. (1.1) with respect to $\boldsymbol{X}$ and employ the chain rule to obtain

$$\ddot{\boldsymbol{J}} + \dot{\boldsymbol{J}} = \nabla \boldsymbol{u} \boldsymbol{J}. \tag{2.4}$$

To derive this equation, we employed $\dot{\boldsymbol{J}} = \partial\dot{\boldsymbol{x}}/\partial\boldsymbol{X}$ and $\ddot{\boldsymbol{J}} = \partial\ddot{\boldsymbol{x}}/\partial\boldsymbol{X}$, which hold true since $\boldsymbol{X} \neq \boldsymbol{X}(t)$. Also, $\nabla\boldsymbol{u}$, which is a short-hand notation for $\partial\boldsymbol{u}/\partial\boldsymbol{x}$, is expressed in terms of $\boldsymbol{x}$ and thus tractable by computing the gradient of fluid velocity along the trajectory of the cloud. The tensor $\nabla\boldsymbol{u}$ is a general function of time and as a result Eq. (2.4) is not a constant coefficient ordinary differential equation (ODE) to be integrated directly. On the other hand, for $\mathcal{C} \neq 0$, $|\boldsymbol{J}|$ exponentially grows or decays indefinitely in time. As discussed in the next section, this exponential variation hinders its accurate numerical computation. In this study we make use of

$$\boldsymbol{F} := \dot{\boldsymbol{J}}\boldsymbol{J}^{-1}, \tag{2.5}$$

a transformation that produces a more tractable constant coefficient ODE with favorable numerical properties. Based on this transformation,

$$\dot{\boldsymbol{F}} = \ddot{\boldsymbol{J}}\boldsymbol{J}^{-1} - \boldsymbol{F}^2 \tag{2.6}$$

and hence from Eq. (2.4)

$$\dot{\boldsymbol{F}} + \boldsymbol{F}^2 + \boldsymbol{F} = \nabla\boldsymbol{u}, \tag{2.7}$$

which classifies as the Riccati equation.

Equation (2.7), in contrast to Eq. (2.4), is nonlinear and has constant coefficients. It is expressed in terms of $\boldsymbol{F}$, which is the instantaneous rate of deformation of the cloud normalized by its size. As a result, its determinant, $|\boldsymbol{F}|$, converges to a non-zero constant for $\mathcal{C} \neq 0$. To show that, we employ Jacobi's formula,

$$\mathrm{tr}(\boldsymbol{F}) = |\boldsymbol{J}|^{-1}\,\frac{\mathrm{d}\,|\boldsymbol{J}|}{\mathrm{d}t}, \tag{2.8}$$

along with Eqs. (2.2) and (2.3) to obtain

$$\mathcal{C} = \overline{\mathrm{tr}(\boldsymbol{F})}, \tag{2.9}$$

in which $\mathrm{tr}(\bullet)$ is the trace operator. This simple relationship indicates that $\mathcal{C}$, which is the sum of the Lyapunov exponents, is the time average of eigenvalues of $\boldsymbol{F}$. In other words, eigenvalues of $\boldsymbol{F}$ are the finite-time Lyapunov exponents associated with the inertial particles pairs. In the following, we solve Eq. (2.7) for $\boldsymbol{F}$ to find an analytical estimate for $\mathcal{C}$ via Eq. (2.9).

Tensor $\nabla\boldsymbol{u}$ is a general function of time. To solve Eq. (2.7) asymptotically, we express $\nabla\boldsymbol{u}$ as a set of harmonic functions using the Fourier transformation. Thus, defining

$$\boldsymbol{G}(\omega) := \frac{1}{2\pi}\int_{-\infty}^{\infty} \nabla\boldsymbol{u}(t)e^{-\hat{i}\omega t}\mathrm{d}t, \tag{2.10}$$

Eq. (2.7) can be written as

$$\dot{\boldsymbol{F}} + \boldsymbol{F}^2 + \boldsymbol{F} = \sum_{\omega} \boldsymbol{G}(\omega)e^{\hat{i}\omega t}. \tag{2.11}$$

Note $\omega \in (-\infty, \infty)$ is implied in all summations without explicit bounds. Next, we consider an asymptotic solution to Eq. (2.11) with the following form

$$\boldsymbol{F} = \lambda\boldsymbol{I} + \sum_{\omega} \boldsymbol{\epsilon}_1(\omega)e^{\hat{i}\omega t} + \sum_{\omega} \boldsymbol{\epsilon}_2(\omega)e^{2\hat{i}\omega t} + \cdots, \tag{2.12}$$

where $\boldsymbol{I}$ is the identity tensor, λ is a representative Lyapunov exponent, and tensor $\boldsymbol{\epsilon}_i(\omega)$ is the i^{th}-order oscillatory response of $\boldsymbol{F}$ to $\boldsymbol{G}$. For a given generic flow, the Lyapunov

exponents are not equal. However, only a representative exponent is considered in Eq. (2.12) because the flow is assumed to be isotropic with no preferred direction and the coordinate system rotation, if any, is assumed to be uncorrelated with the cloud rotation. From Eq. (2.12), $\mathcal{C}$ is directly computed from Eq. (2.9) as

$$\mathcal{C} = N_{\mathrm{sd}}\lambda, \tag{2.13}$$

where N_{sd} denotes the number of spatial dimensions.

Neglecting the higher-order terms in Eq. (2.12), i.e., assuming $\boldsymbol{\epsilon}_i \approx 0$ for all $i > 1$, and substituting it in Eq. (2.11) yields

$$(\lambda+\lambda^2)\boldsymbol{I} + \sum_{\omega}(1+2\lambda+\hat{i}\omega)\boldsymbol{\epsilon}_1(\omega)e^{\hat{i}\omega t} + \sum_{\omega_n}\sum_{\omega_m}\boldsymbol{\epsilon}_1(\omega_n)\boldsymbol{\epsilon}_1(\omega_m)e^{\hat{i}(\omega_n+\omega_m)t} = \sum_{\omega}\boldsymbol{G}(\omega)e^{\hat{i}\omega t}. \tag{2.14}$$

Assuming $|\boldsymbol{\epsilon}_1| \ll 1$, all the time-dependent terms in the second summation can be neglected compared to those in the first summation. The remaining time-independent terms are retained as they might be of the same order of magnitude as the first term. Thus, keeping only the terms with $\omega_n = -\omega_m$ yields

$$(\lambda+\lambda^2)\boldsymbol{I} + \sum_{\omega}\boldsymbol{\epsilon}_1(\omega)\boldsymbol{\epsilon}_1(-\omega) + \sum_{\omega}(1+2\lambda+\hat{i}\omega)\boldsymbol{\epsilon}_1(\omega)e^{\hat{i}\omega t} = \sum_{\omega}\boldsymbol{G}(\omega)e^{\hat{i}\omega t}. \tag{2.15}$$

For Eq. (2.15) to hold,

$$\boldsymbol{\epsilon}_1(\omega) = (1+2\lambda+\hat{i}\omega)^{-1}\boldsymbol{G}(\omega),$$

$$\lambda+\lambda^2 + N_{\mathrm{sd}}^{-1}\sum_{\omega}\mathrm{tr}\left[\boldsymbol{\epsilon}_1(\omega)\boldsymbol{\epsilon}_1(-\omega)\right] = 0. \tag{2.16}$$

From Eq. (2.16)

$$\lambda+\lambda^2 + N_{\mathrm{sd}}^{-1}\sum_{\omega}\frac{\mathrm{tr}\left[\boldsymbol{G}(\omega)\boldsymbol{G}(-\omega)\right]}{(1+2\lambda)^2+\omega^2} = 0. \tag{2.17}$$

Using the convolution theorem, Eq. (2.17) is expressed in terms of a continuous integral as

$$\lambda+\lambda^2 - N_{\mathrm{sd}}^{-1}\int_{-\infty}^{\infty}\frac{\tilde{\rho}^{\mathrm{Q}}(\omega)}{(1+2\lambda)^2+\omega^2}\mathrm{d}\omega = 0, \tag{2.18}$$

where $\tilde{\rho}^{\mathrm{Q}}$ is the Fourier transform of the autocovariance of Q-criterion defined in Eq. (1.4).

Equation (2.18) is the main result of this analysis, which reproduces R-M and S-L expressions exactly. Linearizing Eq. (2.18) at the limit of $|\lambda| \ll 1$ and using Eq. (2.13) to express it in terms of $\mathcal{C}$ exactly reproduce S-L (Eq. (1.3)). Furthermore, neglecting ω^2 in the denominator reduces the integral to $\rho^{\mathrm{Q}}(0) = \overline{\|\boldsymbol{\Omega}\|^2 - \|\boldsymbol{S}\|^2}$, exactly reproducing R-M (Eq. (1.2)). In contrast to the other two expressions, the present result may produce a λ with a non-zero imaginary part. The imaginary part of λ denotes particles crossovers or a cloud turning inside out. Also, the dimensional form of ω in this relationship is normalized by the particle relaxation time τ and becomes larger at larger St. Hence, Eq. (2.18) filters $\tilde{\rho}^{\mathrm{Q}}$ at higher frequencies pertaining to the unresponsiveness of large St particles to flow variations with a small time scale. In the present form, Eq. (2.18) classifies as the Fredholm integral equation of the second kind and its further simplification requires additional assumptions. In the following section, we present an explicit solution for λ for a case in which the underlying flow oscillates at a single frequency.

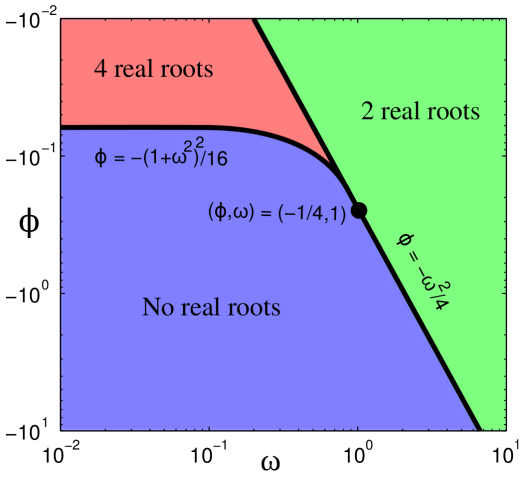

FIGURE 1. The discriminants of Eq. (3.2) and its number of real roots for different values of Φ and ω. There are always two real roots for $\Phi > 0$ (not shown).

3. Single-mode excitation

In this section, we consider the case in which $\tilde{\rho}^{\mathrm{Q}}$ is a single-harmonic oscillatory function of time. This model problem is studied for its importance in revealing the response of Eq. (2.18) to the entire parameter space. This investigation will provide us with a picture of various possibilities that may occur in more complex flows.

For a single-mode excitation, $\tilde{\rho}^{\mathrm{Q}}$ is non-zero at one frequency, i.e.,

$$\tilde{\rho}^{\mathrm{Q}}(\omega') = N_{\mathrm{sd}}\Phi\delta(\omega - \omega'), \tag{3.1}$$

where δ is the Kronecker delta function and Φ is a 1D-equivalent amplitude of the excitation at a single frequency ω. In this case, Eq. (2.18) becomes

$$\lambda + \lambda^2 - \frac{\Phi}{(1+2\lambda)^2 + \omega^2} = 0. \tag{3.2}$$

In total, there are two nondimensional parameters that appear in Eq. (3.2), expressing $\lambda = \lambda(\Phi, \omega)$. Equation (3.1) and consequently Eq. (3.2) also represent multi-dimensional isotropic flows as long as $\tilde{\rho}^{\mathrm{Q}}$ contains only a single frequency.

According to Eq. (3.2), λ is one of the roots of a fourth-order polynomial. Closer examination shows that this equation has two real roots for $\Phi > -\omega^2/4$ or $\Phi > 0$, no real roots for $\Phi < -(\omega^2+1)^2/16$ or $-(\omega^2+1)^2/16 < \Phi < -\omega^2/4$, and four real roots otherwise (Figure 1).

The roots of this system can be analytically computed by converting it to a depressed quadratic form and taking

$$\gamma = 1 + 2\lambda. \tag{3.3}$$

With this change of variable, Eq. (3.2) becomes

$$\gamma^4 + \left(\omega^2 - 1\right)\gamma^2 - 4\Phi - \omega^2 = 0. \tag{3.4}$$

Therefore,

$$\gamma^2 = \frac{1}{2}(1-\omega^2) \pm \frac{1}{2}\sqrt{(\omega^2+1)^2 + 16\Phi}. \tag{3.5}$$

No contraction or expansion is expected in the absence of flow. Thus, $\lambda = 0$ or $\gamma = 1$

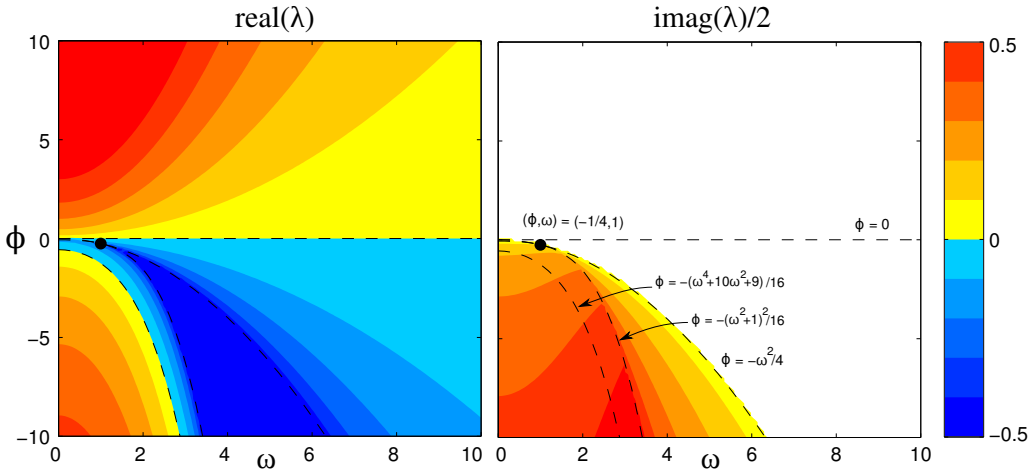

FIGURE 2. The expansion-rate, real(λ), and crossover-rate, imag(λ), of a cloud of particles predicted by Eq. (3.6) as a function of the amplitude Φ and frequency ω of the flow oscillations. Expansion (real(λ) > 0) is predicted in the presence of rotation-rate or strong strain-rate. For $-(\omega^2+1)^2/16 < \Phi < -\omega^2/4$, real($\lambda$) is constant $-1/2$. The crossover-rate is zero everywhere except for the strong-straining flows, in which $\Phi < -(\omega^2+1)^2/16$ or $-(\omega^2+1)^2/16 < \Phi < -\omega^2/4$.

conditions must be satisfied when $\Phi = 0$. Therefore, from the two possible solutions in Eq. (3.5), only the root corresponding to the plus sign is admissible. Computing λ from Eqs. (3.3) and (3.5) and imposing the condition $\lambda(\Phi = 0, \omega) = 0$ lead to

$$\lambda = -\frac{1}{2} + \frac{\sqrt{2}}{4}\sqrt{1 - \omega^2 + \sqrt{(\omega^2+1)^2 + 16\Phi}}. \tag{3.6}$$

Remarks on Eq. (3.6):

(*a*) Equation (3.6) indicates that λ has an imaginary part only in the case of $\Phi < -(\omega^2+1)^2/16$ or $-(\omega^2+1)^2/16 < \Phi < -\omega^2/4$ (blue region in Figure 1). The mean rate of crossovers, represented by imag(λ), is predicted only in low-frequency oscillatory strong-straining flows (Figure 2).

(*b*) The real part of λ represents the expansion-rate (real(λ) > 0) or contraction (real(λ) < 0). Since the second term in Eq. (3.6) is always positive, the strongest possible contraction-rate is $-1/2$. For $\omega < 1$, the minimum value of real(λ) occurs at the discriminant curve $\Phi = -(\omega^2+1)^2/16$, at which real($\lambda$) is not differentiable. For $\omega > 1$, the minimum occurs in a region enclosed between $-(\omega^2+1)^2/16 < \Phi < -\omega^2/4$, where real($\lambda(\Phi, \omega)$) is constant and equal to the global minimum $-1/2$ (Figure 2).

(*c*) No expansion or contraction is predicted for two cases. The first is the trivial case in which $\Phi = 0$. The second case occurs at $\Phi = -(\omega^4 + 10\omega^2 + 9)/16$. In the latter case only real(λ) $= 0$ and imag(λ) $\neq 0$, indicating particle crossovers while of the volume of the cloud is preserved.

(*d*) In the elliptic regions of the flow with $\Phi > 0$, real(λ) > 0 and imag(λ) $= 0$; i.e., clouds of particles always experience pure expansion in the rotation-dominated regimes (Figure 2). Contrary to the contraction-rate, the expansion-rate is unbounded. In general real(λ) is proportional to Φ for $|\Phi| \ll 1$ and to $|\Phi|^{1/4}$ for $|\Phi| \gg 1$.

(*e*) The maximum of imag(λ) occurs at $\Phi = -(\omega^2+1)^2/16$ for $\omega > 1$, at which imag(λ) is not differentiable.

The R-M and S-L expressions can also be simplified for this case using Eq. (3.1). From

Eqs. (1.3), (2.13), and (3.1) S-L prediction in the case of a single-mode excitation is

$$\lambda = \frac{\Phi}{1+\omega^2}. \tag{3.7}$$

Similarly, the R-M relation from Eq. (1.2) becomes

$$\lambda = \Phi. \tag{3.8}$$

As discussed above, these two relationships can also be derived from Eq. (3.6) or Eq. (3.4) under the assumption of $|\lambda| \ll 1$ and $|\omega| \ll 1$. In the following section, we compare the prediction of these three expressions with the reference numerical solution.

4. Numerical validation

To validate the present analysis, we numerically time-integrate Eq. (2.7), which is the linearized form of Eq. (1.1). To replicate a flow condition at which Eq. (3.1) holds, we set $\nabla \boldsymbol{u} = \sqrt{-2\Phi}\cos(\omega t)$. Since this source term is imaginary for $\Phi > 0$, the integration is performed in the imaginary plane. As alluded to earlier, we employ Eq. (2.7) rather than Eq. (2.4) in our computations for its favorable numerical properties, avoiding the ill-conditioning issue that may arise by the exponential growth of $|\boldsymbol{J}|$. To ensure stability and accuracy, we adopt the implicit and second-order Crank-Nicolson time-integration scheme. The implicit time-integration of Eq. (2.7) involves computation of the root-square of a tensor in multiple dimensions, which is accomplished by eigenvalue decomposition of $\boldsymbol{F}$.

For specific combinations of ω and Φ the solution of Eq. (2.7) behaves similar to a chaotic system and becomes very sensitive to the initial condition. $\mathcal{C}$, however, is governed by the time average of $\boldsymbol{F}$ over a long period and is not affected by the initial condition. Hence, we take $\boldsymbol{F}(t=0) = \boldsymbol{I}$. Once $\boldsymbol{F}(t)$ is calculated for any given ω and Φ, $\ln(|\boldsymbol{J}|)$ is calculated from Eq. (2.5) as the time integral of $\boldsymbol{F}$. The behavior of $\ln(|\boldsymbol{J}|)$ as a function of time widely varies depending on ω and Φ (Figure 3). The slope of these curves is equivalent to $\overline{\mathrm{tr}(\boldsymbol{F})}$, which based on Eq. (2.9) is equal to $\mathcal{C}$. Since $N_{\mathrm{sd}} = 1$, this slope is identical to λ (Eq. (2.13)), providing a numerical estimate for it. We refer to the results obtained from this procedure as the numerical solution and use them as a reference for validation of our analysis. These 1D calculations are also repeated at $N_{\mathrm{sd}} = 2$. The results are identical, showing the applicability of Eq. (3.1) to higher-dimensional isotropic flows excited with a single mode.

Following the aforementioned procedure, real(λ) is calculated for $\omega \in [0, 10]$ and $\Phi \in [-10, 10]$ and is shown in Figure 4. This figure shows that real(λ) is a nonlinear function of ω and Φ. For certain combinations of ω and Φ, real(λ) is not differentiable or has a very sharp gradient. There are two primary conclusions that can be drawn based on these results. The first is the possibility of expansion in the strain-dominated hyperbolic regions of the flow, where $\Phi < 0$ and $\lambda > 0$. The second is the existence of a bound on the magnitude of the contraction-rate, which never drops below $-1/2$. While both R-M and S-L fail to make similar predictions, the prediction of the present analysis fully agrees with these observations.

A closer comparison between the reference numerical results (Figure 4) and our analysis (Figure 2) to a large extent confirms the accuracy of our asymptotic solution. Apart from predicting expansion in the presence of strong low-frequency strain oscillations and the existence of a lower bound on the contraction-rate, our analysis correctly predicts real(λ) $\propto |\Phi|^{1/4}$ as $|\Phi| \to \infty$ and real(λ) $\propto \Phi$ when $\Phi \ll 1$. The discriminant curves

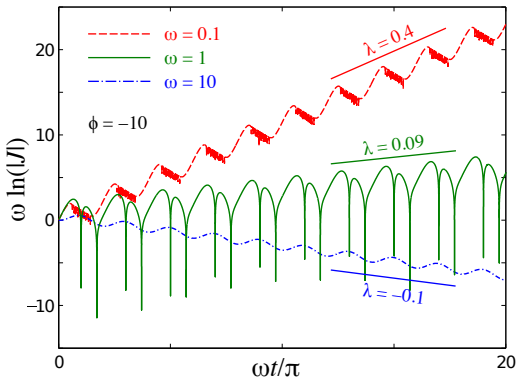

FIGURE 3. The time variation of the volume of a cloud subjected to an oscillatory velocity gradient at three frequencies. Curves are obtained from the direct numerical integration of Eq. (2.7). Our numerical estimate of real(λ) is based on the time-averaged slope of these curves.

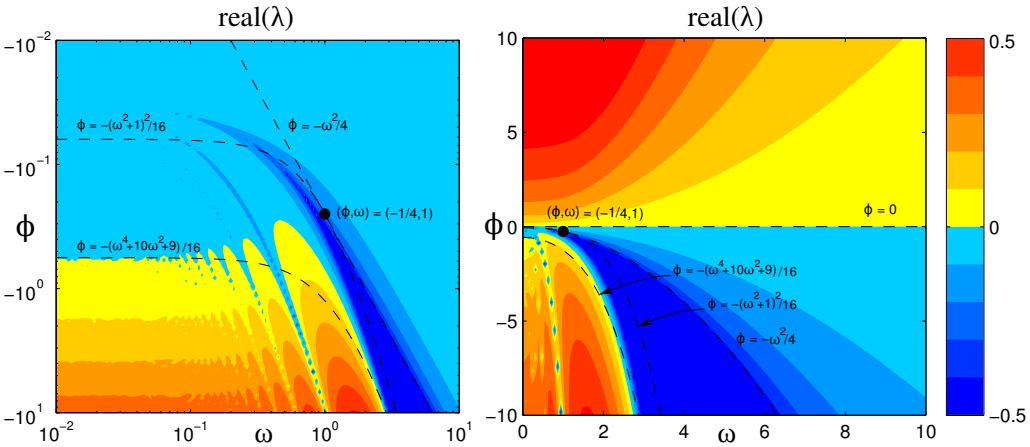

FIGURE 4. The expansion-rate of clouds, real(λ), obtained from the numerical integration of Eq. (2.7) for a flow excited by a single mode (Eq. (3.1)), in log and linear scale as a function of excitation amplitude Φ and frequency ω. Dashed lines are predicted discriminant from our analysis and replicated from Figure 2.

obtained from our analysis provide a good approximation for the values at which the numerical solution changes sign or reaches a plateau. However, discrepancies between the two are also observed, specifically for $\omega \lesssim 1$ and $\Phi \lesssim -1$, i.e., where imag(λ) $\neq 0$ (blue region in Figure 1). While our analysis predicts real(λ) $= -1/2$ for $-(\omega^2+1)^2/16 < \Phi < -\omega^2/4$, the numerical calculation shows the region at which real(λ) $= -1/2$ is larger and includes lower values of Φ. Also, a much higher degree of nonlinearity is observed in the numerical results for $\Phi < -(\omega^4 + 10\omega^2 + 9)/16$.

To explain these discrepancies, it is important to note that Eq. (3.6) is an exact solution of Eq. (2.18) when Eq. (3.1) holds. However, Eq. (2.18) is asymptotically obtained from Eq. (2.7) while neglecting the higher-order terms, i.e., $\boldsymbol{\epsilon}_i$ for $i > 1$. This approximation accounts for the difference between the analytical predictions and the numerical calculations. It can be shown that the rate at which $|\boldsymbol{\epsilon}_i|$ decays as i becomes larger depends on the ratio $|\Phi|/\omega$. Based on the leading order estimates, $|\boldsymbol{\epsilon}_i| \propto (|\Phi|/\omega)^i$ if $|\Phi|/\omega < 1$.

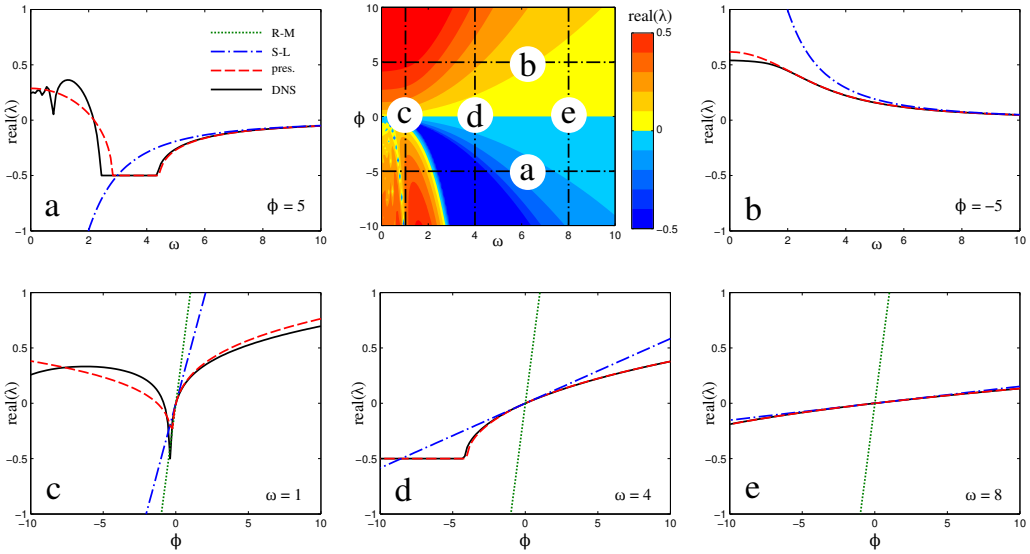

FIGURE 5. The expansion-rate of clouds, real(λ), computed from the numerical calculations (solid black line), the present analysis or Eq. (3.6) (dashed red line), S-L or Eq. (3.7) (dashed–dotted blue line), and R-M or Eq. (3.8) (dotted green line) at different values of ω and Φ. R-M predictions are outside of the depicted range in (a) and (b) and are not shown.

In the worst-case scenario $|\boldsymbol{\epsilon}_1| \approx |\boldsymbol{\epsilon}_2| \approx \cdots \approx |\boldsymbol{\epsilon}_n|$ and the asymptotic form in Eq. (2.12) does not converge.

The S-L prediction of λ, which is a linear function of Φ and a nonlinear function of ω, is completely invalid for $|\Phi|/\omega \gg 1$. In general, S-L provides a good prediction for $\omega \gg 1$ or $|\Phi| \ll 1$. The R-M prediction, on the other hand, which is a linear function of Φ and independent of ω, is valid only for $\omega \ll 1$ and $|\Phi| \ll 1$. These two relations fail to predict main characteristics of real(λ) (Figure 4) such as $\min(\text{real}(\lambda)) \geq -0.5$, real($\lambda$) > 0 for $\Phi \ll -\omega^4$, and real(λ) $\propto |\Phi|^{1/4}$ for $|\Phi| \gg 1$. To highlight these differences, predictions of R-M and S-L relations along with the present analysis are compared against the reference numerical results in Figure 5.

Figure 5(c) confirms R-M and S-L predictions are invalid at small ω, except for $\Phi \ll 1$. These two relations predict real(λ) $= -5$ at $\omega = 0$ and $\Phi = -5$, while real(λ) $= 0.3$ and 0.29 from the numerical calculations and the present analysis, respectively. At higher ω, the S-L prediction approaches the numerical solution, whereas R-M remains inaccurate (Figure 5(e)). The present analysis provides a reasonable approximation at all ω and Φ.

5. Conclusions

An asymptotic solution (Eq. (2.18)) is derived for the expansion-rate of particle clouds. The expansion-rate can be interpreted as the divergence of particle velocity along its trajectory or the sum of Lyapunov exponents associated with particle pairs. We showed that our solution is more general than the expressions provided by Maxey (1987) and Esmaily & Mani (2016), which are valid only under restrictive sets of conditions. Similar to the other two expressions, our solution is related to the underlying flow through the autocovariance of Q-criterion in the Fourier space. We tested these expressions via a case in which the autocovariance function is excited at a single mode. The results showed that

clouds always experience expansion in a rotation-dominated flow, while they may expand or contract in a strain-dominated flow. Our numerical calculations showed that expansion can occur when the strain-rate has a sufficiently large amplitude $|\Phi|$ and sufficiently low frequency ω. These results also showed that the contraction-rate is bounded to $-1/2$. These two major observations, which are a direct consequence of the nonlinear behavior of $\lambda(\Phi, \omega)$, while not captured by the other analyses, are fully predicted by the present analysis. While the previous analyses are valid only in regimes with small Φ or large ω, the present analysis is in good agreement with the numerical results in the entire parameter space. Applying our analysis to complex multi-dimensional flows, in which a continuous range of frequencies are present, remains a subject of future studies.

Acknowledgments

This work was supported by the Department of Energy under the Predictive Science Academic Alliance Program 2 (PSAAP-2) at Stanford University.

REFERENCES

Aliseda, A., Cartellier, A., Hainaux, F. & Lasheras, J. C. 2002 Effect of preferential concentration on the settling velocity of heavy particles in homogeneous isotropic turbulence. *J. Fluid Mech.* **468**, 77–105.

Balachandar, S. & Eaton, J. K. 2010 Turbulent dispersed multiphase flow. *Annu. Rev. Fluid Mech.* **42**, 111–133.

Bec, J., Gawedzki, K. & Horvai, P. 2004 Multifractal clustering in compressible flows. *Phys. Rev. Lett.* **92**, 224501.

Calzavarini, E., Cencini, M., Lohse, D. & Toschi, F. 2008 Quantifying turbulence-induced segregation of inertial particles. *Phys. Rev. Lett.* **101**, 084504.

Dubief, Y. & Delcayre, F. 2000 On coherent-vortex identification in turbulence. *J. Turbul.* **1**, N11.

Eaton, J. K. & Fessler, J. 1994 Preferential concentration of particles by turbulence. *Int. J. Multiphas. Flow.* **20**, 169–209.

Esmaily, M. & Mani, A. 2016 A mathematical analysis of particle clustering in turbulent flows. In *9th International Conference on Multiphase Flow* Firenze, Italy.

Ferry, J., Rani, S. L. & Balachandar, S. 2003 A locally implicit improvement of the equilibrium Eulerian method. *Int. J. Multiphas. Flow.* **29**, 869–891.

Fessler, J. R., Kulick, J. D. & Eaton, J. K. 1994 Preferential concentration of heavy particles in a turbulent channel flow. *Phys. Fluids.* **6**, 3742–3749.

Goto, S. & Vassilicos, J. 2008 Sweep-stick mechanism of heavy particle clustering in fluid turbulence. *Phys. Rev. Lett.* **100** (5), 054503.

Hunt, J. C., Wray, A. A. & Moin, P. 1988 Eddies stream, and convergence zones in turbulent flows. *Proceedings of the Summer Program*, Center for Turbulence Research, Stanford University, pp. 193–208.

Ijzermans, R. H., Meneguz, E. & Reeks, M. W. 2010 Segregation of particles in incompressible random flows: singularities, intermittency and random uncorrelated motion. *J. Fluid Mech.* **653**, 99–136.

Maxey, M. 1987 The gravitational settling of aerosol particles in homogeneous turbulence and random flow fields. *J. Fluid Mech.* **174**, 441–465.

Ray, B. & Collins, L. R. 2011 Preferential concentration and relative velocity statistics

of inertial particles in Navier–Stokes turbulence with and without filtering. *J. Fluid Mech.* **680**, 488–510.

Robinson, A. 1956 On the motion of small particles in a potential field of flow. *Commun. Pur. Appl. Math.* **9**, 69–84.

Salazar, J. P., De Jong, J., Cao, L., Woodward, S. H., Meng, H. & Collins, L. R. 2008 Experimental and numerical investigation of inertial particle clustering in isotropic turbulence. *J. Fluid Mech.* **600**, 245–256.

Saw, E. W., Shaw, R. A., Ayyalasomayajula, S., Chuang, P. Y. & Gylfason, A. 2008 Inertial clustering of particles in high-Reynolds-number turbulence. *Phys. Rev. Lett.* **100**, 214501.

Tagawa, Y., Mercado, J. M., Prakash, V. N., Calzavarini, E., Sun, C. & Lohse, D. 2012 Three-dimensional Lagrangian Voronoi analysis for clustering of particles and bubbles in turbulence. *J. Fluid Mech.* **693**, 201–215.